NJC

Cite this: *New J. Chem.*, 2012, **36**, 2506–2513

www.rsc.org/njc

PAPER

Bis-silylated terephthalate as a building block precursor for highly fluorescent organic–inorganic hybrid materials†

Daniela Pletsch, Fabiano da Silveira Santos, Fabiano Severo Rodembusch, Valter Stefani* and Leandra Franciscato Campo*

Received (in Montpellier, France) 25th May 2012, Accepted 14th September 2012
DOI: 10.1039/c2nj40434f

A bis-silylated diethyl 2,5-bis[*N*,*N*-(3-triethoxysilyl)propylurea]terephthalate precursor (**5**) was synthesized from a terephthalate derivative (**3**) and successfully used to prepare highly fluorescent organosilicas by hydrolytic self-condensation (**DPM1**) and co-condensation (**DPM2**) with tetraethoxysilane. The dyes **3** and **5** present absorption in the UV-Vis region and fluorescence emission in the yellow and blue regions, respectively. The red-shifted bands in the absorption spectra of dye **3** with respect to dye **5** can be related to the formation of intramolecular charge transfer (ICT) state even in the ground-state due to the strong electron-donor amino groups and moderate electron-withdrawing carbonyl groups present in the benzenic ring. The small Stokes' shift, as well as the high fluorescence quantum yield values discards the intramolecular proton transfer mechanism in the excited state. The fluorescence emission dependence on the solvent polarity indicates that an intramolecular charge transfer (ICT) or a locally excited (LE) state is taking place in the excited state to the dyes **3** and **5**, respectively. The new fluorescent hybrid materials (**DPM1** and **DPM2**) show absorption maxima in the solid state located at around 390 nm, indicating that the electronic structure of the fluorescent precursor was not significantly perturbed in the ground state after its self-condensation or co-condensation with TEOS. The fluorescent material **DPM2** presents a photophysical behavior quite similar to the precursor in solution. On the other hand, the self-condensed material **DPM1** presents a fluorescence emission maximum red-shifted by 33 nm, which can be probably attributed to π–π stacking between the terephthalate cores. Any evidence of auto-organization could be observed in these materials.

Introduction

The incorporation of photoresponsive precursors into the sol–gel matrix as organic building blocks can be a powerful tool for developing new fluorescent organosilicas for optical applications such as photostabilizers, waveguides, laser materials, and organic light emitting diodes (OLEDs).[1–10] In particular, self-assembly of bridged silsesquioxanes represents a typical and efficient approach to design and fabricate silica-based hybrid materials based on a sol–gel process.[11] The concept of self-directed assembly in sol–gel derived bridged silsesquioxane hybrid materials was first presented by Moreau *et al.*,[12] where new hybrid materials were reported with helical morphology *via* H-bond mediated hydrolysis of a single chiral precursor. A left- or right-handed helix was auto-generated, according to the configuration of the organic substructure. Since then several bridged silsesquioxanes with photoluminescent properties have been published.[13–16] All the molecular organic precursors containing at least two alcoxysilyl groups can be transformed into nanostructured hybrid materials by hydrolytic sol–gel polycondensation.[17] A wide variety of organic functionalities can be incorporated into the silica network,[18] including alkyl, aromatic, heterocyclic groups, chelating systems (cyclames, crown ethers, porphyrins, *etc.*), chiral molecules,[19,20] as well as polymers.[2,9,21] The most common self-organization of organic units can be obtained by van der Waals interactions, for example π–π interaction between the aromatic rings and/or by intermolecular H-bonding, such as ureido groups between organic groups.

In this work, we present the synthesis and photophysical characterization of a new bridged silsesquioxane with a planar structure due to intramolecular H-bonding in combination with core-to-core intermolecular H-bonding associated with ureido groups.[22,23] The new fluorescent silsesquioxane was used to produce photoresponsive organic–inorganic hybrid materials *via* hydrolytic self-condensation and co-condensation with tetraethoxysilane (TEOS), which can be very interesting

---

Universidade Federal do Rio Grande do Sul, Instituto de Química, Laboratório de Novos Materiais Orgânicos, Av. Bento Gonçalves, 9500. CP 15003, CEP 91501-970, Porto Alegre-RS, Brazil. E-mail: vstefani@iq.ufrgs.br, campo@iq.ufrgs.br; Fax: +55-51-33087304; Tel: +55-51-33087206

† Electronic supplementary information (ESI) available. See DOI: 10.1039/c2nj40434f

since fluorescent terephthalates have received much attention due to their applications in electronic materials, light-emitting diodes (LEDs), and optical sensors.[24–31]

Experimental

Materials and methods

All the solvents and reagents were used as received or purified using standard procedures.[32] Spectroscopic grade solvents (Merck or Aldrich) were used for fluorescence emission and UV-Vis absorption measurements. The compound 1,4-cyclohexanedione-2,5-dicarboxylate (**1**) was synthesized according to the literature.[33] Elemental analyses were performed by Perkin–Elmer model 2400. Melting points were measured using a Gehaka PF 1000 apparatus and are uncorrected. Infrared spectra were recorded using a Shimadzu Prestige 21 in KBr pellets or in ATR mode. ^{1}H and ^{13}C-NMR spectra were performed using a VARIAN INOVA YH300 using tetramethylsilane (TMS) as the internal standard and $CDCl_3$ (Aldrich) as the solvent at room temperature. UV-Vis absorption spectra were performed on a Shimadzu UV-2450 spectrophotometer. Steady state fluorescence spectra were measured using a Shimadzu spectrofluorometer model RF-5301PC. Spectrum correction was performed to enable measuring a true spectrum by eliminating instrumental response such as wavelength characteristics of the monochromator or a detector using Rhodamine B as an external standard (quantum counter). All experiments were performed at room temperature in a concentration of 10^{-5} M. The diffuse reflectance spectra were measured using an ISR-2200 Integrating Sphere Attachment. For the measurements in the solid state, the hybrid materials were treated as powder. The experiments were performed at room temperature and the baseline in the solid-state was obtained using $BaSO_4$ (Wako Pure Chemical Industries, Ltd.). The quantum yields of fluorescence (Φ_{fl}) in solution were determined at 25 °C using the optically dilute method (absorbance lower than 0.05) with anthracene (Φ_{fl} = 0.29)[34] and fluorescein (Φ_{fl} = 0.79)[35] in ethanol as quantum yield standards for the dyes **3** and **5** respectively. Sodium salicylate (Φ_{fl} = 0.42) was used as a quantum yield standard in the solid-state.[36] Time-resolved fluorescence measurements were made by time-correlated, single-photon counting using an EasyLife V spectrophotometer at 22 °C. To the dyes **3** and **5**, excitation wavelengths of 405 and 380 nm, respectively, were applied using a fast laser diode (Table S2, ESI†). The fluorescence emissions from **3** and **5** were isolated from scattered laser light using a rejection filter at 400 and 380 nm, respectively. The chi-squared (χ^2) statistics were about one and randomness in the fit residuals was obtained. Scanning electron microscopy (SEM) was performed using a JEOL LSM 5800 microscope with 20 kV and 850 times of magnification (Fig. S11 and S12, ESI†). Samples were fixed on carbon tape on a stub, followed by gold sputtering. TGA analyses were conducted using a Universal Analyzer V2.6D (TA Instruments). Dry samples, 3–4 mg, were directly weighed into aluminum pans. A heating rate of 20 °C min^{-1} was maintained from 0 to 700 °C with a nitrogen purge. X-ray diffraction patterns of the powdered samples were obtained using a Siemens Diffractometer model D500 using CuKα as a radiation source, λ = 0.15418 nm. The distances were calculated using the Bragg equation. In order to correlate the X-ray patterns with the dye structures, calculations were performed employing the Gaussian 03 software[37] and MOPAC93 packages. A simple conformational analysis was carried out at the semiempirical level (PM3 parametrization) for the precursor (Fig. S8, ESI†).

Synthesis of the fluorescent terephthalates

The terephthalate derivative **3** was prepared as already presented in the literature.[38] The silsesquioxane **5** was prepared according to Fig. 1. In a typical experiment, a suspension of 5.12 g (20 mmol) of diethyl 2,5-dioxocyclohexane-1,4-dicarboxylate (**1**) in 150 mL of glacial acetic acid was heated to 40 °C followed by addition of 4.76 g (44 mmol) of phenylhydrazine (**2**). The solution, initially colorless, became yellow to a dark brown upon addition of phenylhydrazine. The final dark brown solution was mixed for 2 h, diluted in distilled water and extracted three times with dichloromethane. After drying the organic phase with sodium sulphate, the solution was concentrated and the diethyl 2,5-diaminoterephthalate (**3**) was precipitated with cyclohexane and purified by column chromatography eluted with $CHCl_3$ as the solvent. To a solution of 252 mg (1 mmol) of **3** in ethyl acetate (10 mL) was added 800 μL (3.16 mmol) of 3-(triethoxysilyl)propylisocyanate (**4**) and the solution was heated at reflux for 20 h. The diethylterephthalate (**5**), which precipitates into the reaction mixture, was filtered, washed with hexane and dried at room temperature. No additional purification was needed.

Diethyl 2,5-diaminoterephthalate (3). Yield 40%; light yellow needles; m.p. 167–169 °C. Found in the literature: 165–167 °C.[38] ^{1}H NMR (300 MHz, $CDCl_3$): δ (ppm) = 7.20 (s, 2H, H_2 and H_5); 4.85 (broad s, 4H, NH_2); 4.31 (q, 4H, H_8, J = 7.2 Hz); 1.36 (t, 6H, H_9, J = 7.2 Hz). FTIR (cm^{-1}, KBr): 3463 (ν_{as} NH_2), 3366 (ν_s NH_2), 2996 ($\nu_{aliphatic}$ C–H), 1681 (ν C=O), 1580 ($\nu_{aromatic}$ C=C), 1212 (ν C–O–C).

Diethyl 2,5-bis[*N*,*N*-(3-triethoxysilyl)propylurea]terephthalate (5). Yield 70%; m.p. 236–238 °C. Anal. calcd. for $C_{32}H_{58}N_4O_{12}Si_2$ (776.36 g mol^{-1}): C 51.45; H 7.83; N 7.50 (%). Found: C 50.31;

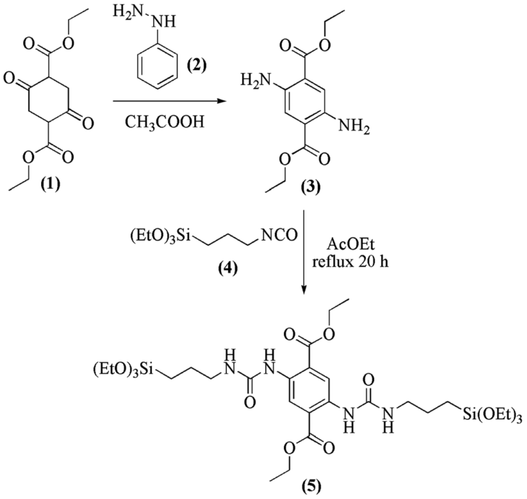

Fig. 1 Synthesis of the terephthalates (**3**) and (**5**).

H 7.70; N 7.49 (%). ^{1}H NMR (300 MHz, $CDCl_3$): δ (ppm) = 10.05 (s, 2H, NH); 9.16 (s, 2H, H_5 and H_2); 5.00 (broad s, 2H, NH); 4.40 (q, 4H, H_8, J = 6.9 Hz); 3.86 (q, 12H, H_{14}, J = 6.9 Hz); 3.40–3.25 (m, 4H, H_{11}); 1.81–1.61 (m, 4H, H_{12}); 1.44 (t, 6H, H_9, J = 6.6 Hz); 1.26 (t, 18H, H_{15}, J = 6.3 Hz); 0.71 (t, 4H, H_{13}, J = 7.8 Hz). ^{13}C NMR (75 MHz, $CDCl_3$): δ (ppm) = 168 (C7); 155 (C10); 136 (C3 and C6); 122 (C2 and C5); 119 (C1 and C4); 62 (C8); 59 (C14); 43 (C11); 23 (C12); 18 (C15); 14 (C9); 8 (C13). FTIR (cm^{-1}, KBr): 3295 (ν NH), 3092 ($\nu_{aromatic}$ C–H), 2965 ($\nu_{aliphatic}$ C–H), 1708 (ν_{ester} C=O), 1646 (ν_{urea} C=O), 1574 ($\nu_{aromatic}$ C=C), 1102 (ν C–O–C).

Synthesis of the hybrid materials. The hydrolysis-polycondensation of **5** allowed the formation of polysilsesquioxanes prepared in the absence (**DPM 1**) or in the presence (**DPM 2**) of TEOS using HCl as catalyst (Fig. 2).

General procedure for the synthesis of xerogel (DPM1). To a solution of 156 mg (0.21 mmol) of **5** and THF (1.4 mL) was added 0.083 mL of the catalyst HCl (0.5 M) and water (1.4 mL) and the mixture was kept under stirring at 60 °C for 4 days. The obtained solid (116 mg), which precipitates in solution, was washed several times with ethanol, acetone, ethyl ether and dried under vacuum for 6 h to give pale yellow powder namely **DPM1**. FTIR (cm^{-1}, KBr): 3320 (ν SiO–H), 2980 ($\nu_{aliphatic}$ C–H), 1716 (ν_{ester} C=O), 1665 (ν_{amide} C=O), 1100 (ν Si–O–Si).

General procedure for the synthesis of xerogel (DPM2). To a solution of 200 mg of **5** (0.27 mmol) and 1.58 g (7.58 mmol) of TEOS in DMSO (3.66 mL) was added 0.172 mL of water and 0.14 mL of the catalyst HCl (0.5 M). The mixture was kept under static conditions at room temperature (25 °C). After ageing the gel for fifteen days, it was powdered, washed several times with ethanol, acetone, ethyl ether and dried under vacuum for 6 h to give pale yellow powder (517 mg) namely **DPM2**. FTIR (cm^{-1}, KBr): 3422 (ν SiO–H), 1646 ($\nu_{ester\ and\ amide}$ C=O), 1062 (ν Si–O–Si).

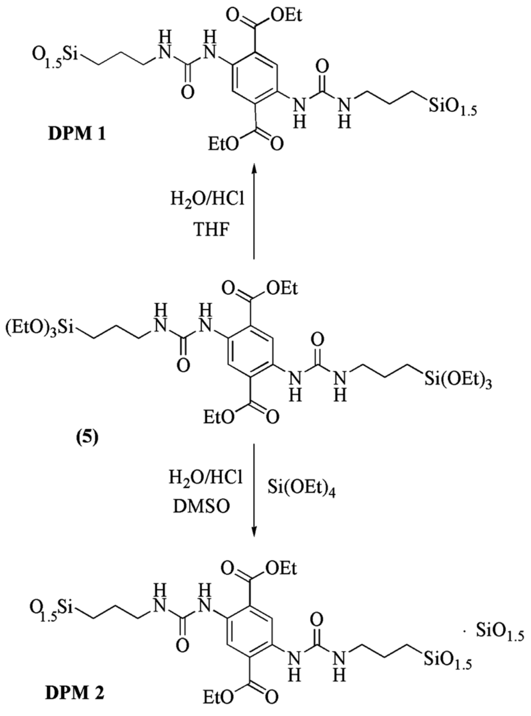

Fig. 2 Preparation of materials **DPM1** and **DPM2**.

Results and discussion

Photophysical characterization

Fig. 3 presents the normalized absorption of the fluorescent dyes in different organic solvents and the relevant photophysical data are summarized in Table 1. The terephthalates **3** and **5** show a main absorption band (λ_{abs}) located at around 435 nm and 386 nm, respectively. The molar extinction coefficient values (ε_{max}) are in agreement with $^1\pi\pi^*$ transitions. The large difference in the location of the absorption maxima between these dyes ($\sim$50 nm) could not be related only to the amino group derivatization, which leads to changes in the electronic distribution in the molecule. The red-shifted bands in the absorption spectra of dye **3** with respect to dye **5** can also be related to the formation of intramolecular charge transfer (ICT) state even in the ground-state due to the strong electron-donor amino groups (–NH_2) and moderate electron-withdrawing carbonyl groups (–C=O) present in the benzenic ring. Thus, spectroscopic bands are drastically affected by the solvent nature.

At this point it is worth mentioning that the terephthalate core was chosen as a building block for preparing hybrid materials not only by the two amino moieties, which allowed us to obtain bis-silylated materials, but also due to the ability to lead proton transfer in the excited state (ESIPT).[40] Concerning this phototautomerism in the excited state, it is well understood that the main conditions for the ESIPT to occur are the presence of an intramolecular hydrogen bond (IHB) between the H atom of the donor group (–OH, –NH_2 or –NHR) and the acceptor (–N= or carbonyl) (intrinsic

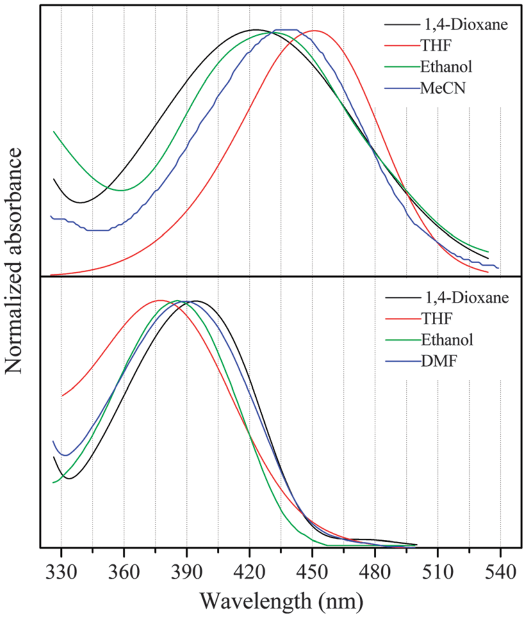

Fig. 3 Normalized absorption spectra of **3** (top) and **5** (bottom) in different organic solvents [10^{-5} M].

Table 1 UV-Vis absorption, fluorescence emission and excitation data of the dyes **3** and **5**, where λ_{abs} is the absorption maxima, λ_{ex} is the excitation maxima and λ_{em} is the fluorescence emission maxima in nanometers, ε is the molar extinction coefficient in 10^4 L mol^{-1} cm^{-1}, Φ_{fl} is the fluorescence quantum yield and $\Delta\lambda_{ST}$ is the Stokes' shift in nm/cm^{-1}

Dye	Solvent	λ_{abs} (ε)	λ_{ex}	λ_{em}	$\Delta\lambda_{ST}$	Φ_{fl}
3	1,4-Dioxane	423 (0.60)	452	488	65/3149	0.80[a]
	THF	448 (4.42)	465	547	99/4040	0.63[a]
	Ethanol	433 (6.10)	446	564	131/5364	0.35[a]
	MeCN	437 (6.75)	451	546	109/4568	0.50[a]
5	1,4-Dioxane	393 (0.72)	408	471	78/4214	0.85[b]
	THF	379 (2.73)	411	469	90/5063	0.66[b]
	Ethanol	385 (1.30)	382	474	89/4877	0.73[b]
	DMF	388 (5.60)	408	473	85/4632	0.77[b]

[a] Fluorescein (λ_{abs} = 429 nm) as the fluorescence quantum yield standard. [b] Anthracene (λ_{abs} = 375 nm) as the fluorescence quantum yield standard.

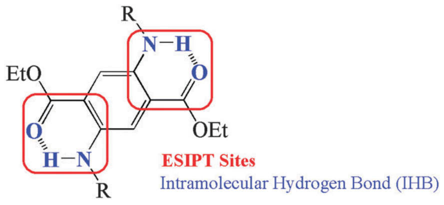

(3) R = H
(5) R = -C(O)NH(CH$_2$)$_3$Si(OEt)$_3$

Fig. 4 Intramolecular hydrogen bond sites in the terephthalate core.

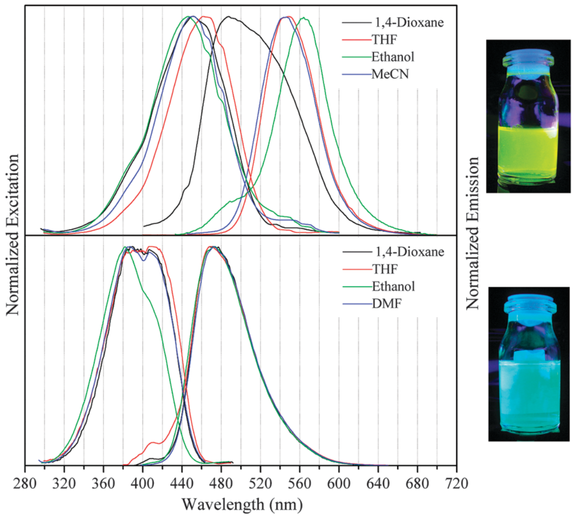

Fig. 5 Normalized fluorescence emission and excitation spectra of **3** (top) and **5** (bottom) in different organic solvents [10^{-5} M]. The pictures of the respective dyes in THF solutions and under UV radiation (365 nm) were also presented.

intramolecular transfers) in the ground state.[39] The terephthalates **3** and **5** present two donor centers (–NH$_2$ or –NHR, respectively) which can form IHB with the acceptor center (–C=O) (Fig. 4). The photophysical characteristics of ESIPT dyes is mainly based on the large Stokes' shift (higher than 6000 cm^{-1})[40] and readily backward proton transfer in the ground state after fluorescence emission, although recent papers have been discussing the ESIPT mechanism with smaller Stokes's shift.[41,42]

The fluorescence emission and excitation spectra of the terephthalates **3** and **5** are shown in Fig. 5. The dye **3** presents one main emission band located at 488–564 nm depending on the solvent, with no overlap of the absorption and fluorescence spectra, suggesting that photo-excitation induced large structural changes[26] or charge redistribution in the excited state.[43] The ability to form an intramolecular hydrogen bond, as well as the significative difference between absorption and emission maxima, suggest that the large structural change could be related to the ESIPT mechanism. However, the fluorescence quantum yields are quite far from the values usually observed to ESIPT dyes.[44–48]

Additionally, although the emission maxima shift with the solvent, it could not be observed a tendency concerning the increase of the solvent polarity/emission maxima location. Such a solvatochromic effect in the emission maxima of **3** can be associated with changes in the excited state charge's distribution as compared to that in the ground state. In more polar aprotic media, the species with charge separation (ICT state) may become the lowest energy state. In a less polar solvent the species without charge separation, the so-called locally excited (LE) state, may have the lowest energy. In this way, the role of the solvent polarity is not only to lower the energy of the excited state due to general solvent effects, but also to govern which state has the lowest energy.[49–51]

Dye **3** in 1,4-dioxane presents a broad blue-shifted band located at 488 nm with a small Stokes shift (3149 cm^{-1}), which can be related to the locally excited state. In this less polar solvent, the ICT state is not favored, and the band position is similar to that observed to dye **5**, which is not practically affected by the polarity of the solvent. The significative difference in the emission maxima between 1,4-dioxane and acetonitrile provides important evidence for some charge transfer character in the excited species, which can probably be related with the amino and carbonyl groups at the *ortho*-positions of the terephthalate core.[41] An observation at the ICT (~536 nm) and the locally excited emissions (488 nm) give two distinct spectra, with excitation maxima at around 452 nm and 427 nm, respectively (Fig. S13 and S14, ESI†). This photophysical feature indicates that the fluorescence emission band originates from at least two different species in the ground state and the absorption spectrum of this dye is a mixture of these species in the ground state.

The dye **5** presents a main emission band located at 470 nm with no solvatochromic effect and a relative large Stokes' shift (4214–5063 cm^{-1}). These results indicate that the derivatization of the amino group to the ureido one seems to play a major role in the photophysics of these dyes, where the substitution of the strongly electron-donor –NH$_2$ moiety by the ureido reduces the electron-donor capacity of the nitrogen atom due to the electron-withdrawing nature of the carbonyl group that ICT cannot occur. Therefore, emission bands practically are unaffected by the solvents (typical for π–π* transitions). It is worth mentioning that although the fluorescence emission is less affected by the solvent polarity, since the ICT state no longer takes place in the excited state, the Stokes' shift remains higher and could even be related to an ESIPT mechanism;[41,42] however, one more time the high values for

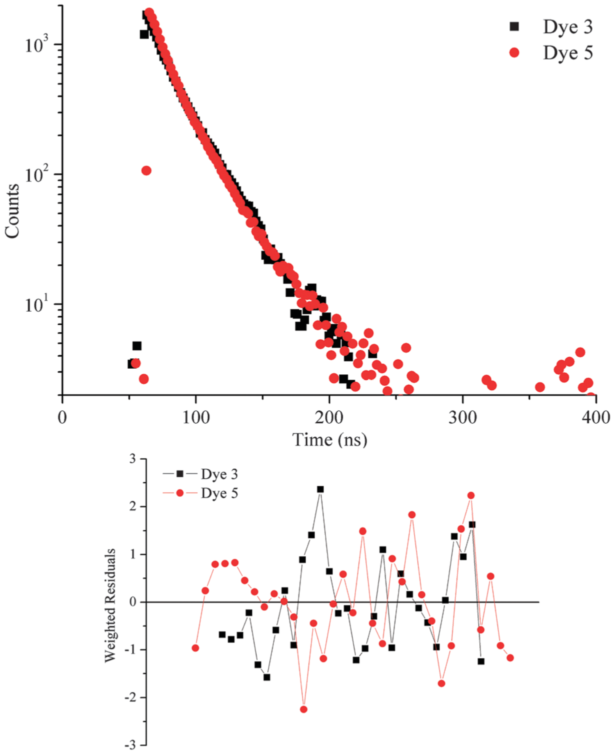

Fig. 6 Fluorescence response functions of dye **3** (black) and dye **5** (red) in 1,4-dioxane at room temperature. The LE and the ICT decays for the dye **3** are analyzed simultaneously (global analysis) to fit a dual exponential decay function. Weighted residual is also presented.

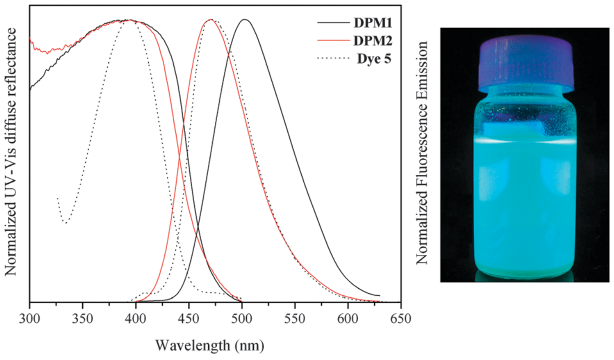

Fig. 7 Normalized UV-Vis diffuse reflectance (left) and fluorescence emission (right) of the fluorescent materials. The UV-Vis and fluorescence emission of dye **5** in 1,4-dioxane is also presented for comparison. The picture of the **DPM2** after gelation and under UV radiation (365 nm) was also presented.

Table 2 Photophysical properties measured using a front face solid sample holder for packed powder samples of **DPM1** and **DPM2**, where λ_{abs} is the absorption maxima, λ_{em} is the fluorescence emission maxima in nanometers, Φ_{fl} is the fluorescence quantum yield and $\Delta\lambda_{ST}$ is the Stokes' shift in nm/cm^{-1}

Material	$\lambda_{abs}{}^{a}$	$\lambda_{em}{}^{b}$	$\Delta\lambda_{ST}$	$\Phi_{fl}{}^{c}$
DPM1	390	504	114/5799	0.02
DPM2	394	471	77/4149	0.15

[a] Absorption maxima were measured using an integrating sphere. [b] Emission maxima upon irradiation at absorption (λ_{exc} = 390 nm). [c] The relative fluorescence quantum yield was determined with sodium salicylate (λ_{exc} = 370 nm).

the fluorescence quantum yields clearly indicate that the emission is probably related to a locally excited state in spite of the lower values expected for the ESIPT tautomer,[44–47] although the mechanism of the energy loss in the excited state still remains unknown. The full width at half the maximum height (fwhm) of the fluorescence band of dye **5** is practically invariant in all studied solvents suggesting that not much change is occurring in the geometry of the molecule on excitation to the excited state.[39]

The time resolved fluorescence emission was performed to the dyes **3** and **5** in 1,4-dioxane (Fig. 6), where a single exponential decay could be observed to the dye **5** (9.29 ns). On the other hand, the experimental results for dye **3** could be fitted by a dual exponential decay, where a fast fluorescence decay (0.046 ns), which could be related to the LE state, followed by a slower one (15.06 ns) could be measured. The relevant data from this experiment are presented in Table S3 (ESI†).

In Fig. 7 are presented the photophysical study in the solid state of the obtained materials. The relevant data of **DPM1** and **DPM2** are summarized in Table 2. In the solid state, the fluorescent materials present absorption maxima located at around 390 nm, which are quite similar to those obtained to the silsesquioxane **5** in solution, indicating that the electronic structure of the fluorescent precursor was not significantly perturbed in the ground state after its self-condensation (**DPM1**) or co-condensation with TEOS (**DPM2**). However, the fluorescence emissions display notable differences between the final materials. The co-condensation with TEOS allowed in obtaining an environment to the fluorescent dye **5**, which is quite similar to the solution. On the other hand, the self-condensed material **DPM1** presents a fluorescence emission maximum red-shifted by 33 nm if compared with **DPM2**, which can be probably attributed to π–π stacking between the terephthalate cores. The obtained materials **DPM1** and **DPM2** exhibit a weak yellow emission in a solid state and present low fluorescence quantum yields when compared with the precursor **5** in solution. Moreover the fluorescence quantum yield for **DPM1** is significantly lower than the obtained for **DPM2**. The excited state deactivation is presumably due to nonradiative decay between the fluorophore with the inorganic network in spite of the radiative pathways. Additionally, according to recently published work concerning the terephthalate derivatives, the quantum yields of pure powder dyes in a solid state were measured and compared to the dyes in solution and the authors found a decrease of this property in the solid state, unless the dyes exhibit an aggregation-induced emission (AIE).[24,26]

It is worth mentioning that broader fluorescence emission curves (fwhm > 100 nm)[13,15] were described for similar silica hybrid materials, which could be related to two emission components. Since the materials prepared in this work present fwhm ~80 nm, the contribution of oxygen-related defects in the siliceous skeleton and electron–hole recombination in the urea groups cannot be discharged for the fluorescence emission.

FTIR characterization

The FTIR spectral features of the materials **DPM1** and **DPM2**, as well as the silsesquioxane **5** are shown in Fig. 8. Concerning the dye **5** and the self-condensed material **DPM1**, both spectra showed bands due to ureido (3300 cm^{-1}), propyl (2970, 2920 and 2880 cm^{-1}), and the carbonyl groups (1700 and 1640 cm^{-1} to ester and amide respectively). Additionally, the **DPM1** displayed stretching bands of the siloxane network (Si–OH at 3400 cm^{-1} and Si–O–Si at 1100 and 1070 cm^{-1}). On the other hand, the **DPM2** shows only the bands related to the inorganic network, as expected.

The FTIR spectra of **DPM1** and **DPM2** (Fig. 8) were used for the determination of the so-called amide I and amide II bands, as already presented in the literature.[13] The 1800–1500 cm^{-1} interval is dominated by a large amide I band at around 1660 cm^{-1} and a sharp amide II band centered at 1550 cm^{-1} (Fig. 9). For both materials, the amide II band, which is mainly associated with the N–H in-plane bending vibration,[13] is more intense than the amide I band. For **DPM1**, the curve-fitting performed for the amide II band was resolved into two individual components at 1564 cm^{-1} (fwhm = 49 cm^{-1}) and 1545 cm^{-1} (fwhm = 50 cm^{-1}), suggesting the formation of hydrogen-bonded aggregates with two distinct degrees of order. Otherwise, for **DPM2** only one component at 1551 cm^{-1} (fwhm = 56 cm^{-1}) was done by curve-fitting of the amide II band, suggesting that in this material, the co-condensation of dye **5** with TEOS leads to a distancing of N–H and C=O groups and therefore, the probability to form hydrogen-bonds diminishes.

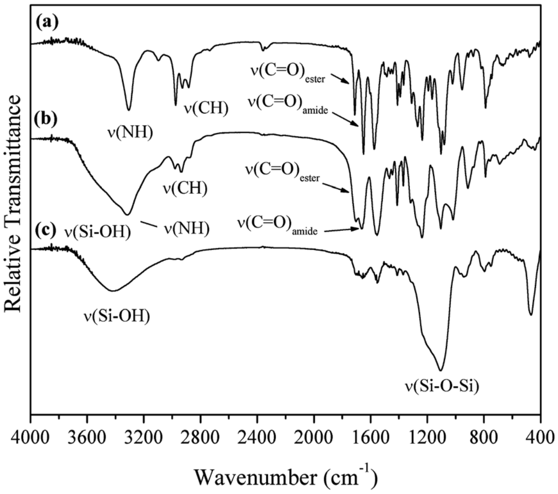

Fig. 8 The FTIR spectra of (a) dye **5**, (b) **DPM1** and (c) **DPM2**.

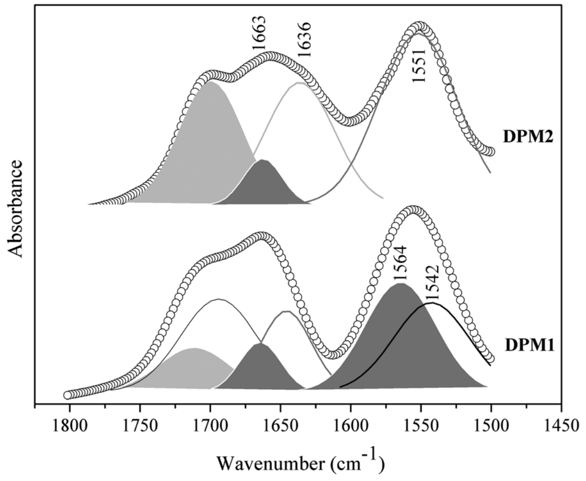

Fig. 9 Curve-fitting results in the amide I and amide II regions of the hybrid materials **DPM1** and **DPM2**.

The amide I band of **DPM1** was decomposed into four components situated at 1712 (fwhm = 48 cm^{-1}), 1694 (fwhm = 53 cm^{-1}), 1663 (fwhm = 28 cm^{-1}) and 1646 cm^{-1} (fwhm = 35 cm^{-1}). In the case of the **DPM2** material the amide I was decomposed into three components at 1700 (fwhm = 45 cm^{-1}), 1663 (fwhm = 27 cm^{-1}) and 1636 cm^{-1} (fwhm = 49 cm^{-1}). The 1712–1694 cm^{-1} interval is attributed to free C=O groups and the band at 1663 cm^{-1} is assigned to the absorption of hydrogen-bonded C=O groups in disordered amide–amide aggregates. Finally, the bands at 1646 and 1636 cm^{-1} for **DPM1** and **DPM2**, respectively, are ascribed to the absorption of C=O groups included in significantly more ordered hydrogen-bonded amide–amide associations.

It is worth mentioning that these spectroscopic results of **DPM1** suggest that it does not occur at an effective condensation of the dye **5**. The results from thermogravimetric analysis (Fig. S15, ESI†) corroborate with this affirmation, where a similar decomposition profile could be observed between dye **5** and **DPM1**, as well as a higher decomposition temperature to the organic portion in the hybrid material (310 °C) in spite of the dye 5 (267 °C).

X-ray characterization

In Fig. 10 is depicted the X-ray diffraction patterns of dye **5**. It can be observed two main patterns located in the scattering vector regions 2.44 and 7.38 nm^{-1}. The intense peak at 2.44 nm^{-1} (d = 2.57 nm) can be related to the C–C distance between the carbon atoms from the ethoxy groups bounded to the silicon atoms (*ca.* 2.68 nm from theoretical calculations see ESI†). On the other hand, the attribution of the less intense peak at 7.38 nm^{-1} (d = 0.85 nm) is not so clear, since two different sites in the structure could fit with the experimental

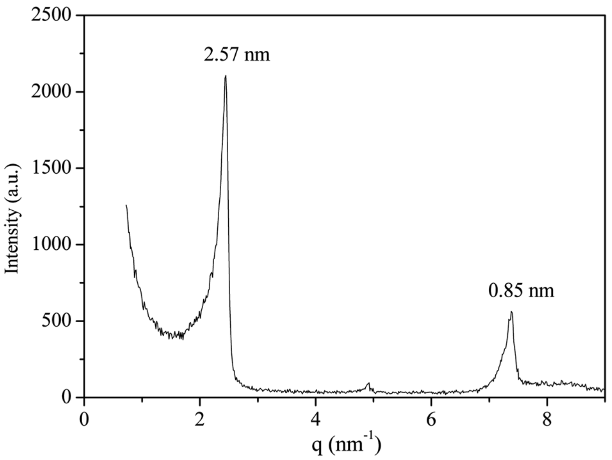

Fig. 10 X-ray diffraction patterns of the silsesquioxane **5**.

data: (i) the distance between the oxygen atoms from the two ester (*ca.* 0.74 nm) or (ii) the distance between the two carbonyl groups from the urea moieties (*ca.* 0.76 nm). It could not be possible to obtain X-ray diffraction patterns related to organization in nanometric level from the materials. A broad and weak peak located at 3.96° and 6.24° for the materials **DPM1** and **DPM2** could be observed, respectively (Fig. S9 and S10, ESI†). The observed X-ray patterns indicate an absence of organization in the material, although the silsesquioxane **5** presents hydrogen bond formation ability, the ester groups play a fundamental role in the precursor organization does not allow specific interactions leading to organization at the nanometric level.

Conclusions

The present study leads to the following conclusions: (i) a fluorescent terephthalate derivative was successfully obtained and derivatized in order to obtain a silsesquioxane precursor to prepare fluorescent organic–inorganic hybrid materials; (ii) the dye **3** shows typical absorption in the UV-Vis region and a fluorescence band in the yellow region due to ICT states, which are very dependent on the solvent polarity due to the strong electron-donor amino groups and moderate electron-withdrawing carbonyl groups present in the benzenic ring; (iii) the substitution of the strongly electron-donor amino group by the –NH–C=O– group the electron-donor capacity is reduced due to the electron-withdrawing nature of the carbonyl group prevents the formation of ICT state. Therefore, emission bands practically are unaffected by the solvent polarity; (iv) the dye **3** presents one main emission band located at a blue-yellow region with no overlap of the absorption and fluorescence spectra, suggesting that photo-excitation induced large charge redistribution in the excited state, which can be related to an ICT state; (v) the new fluorescent hybrid materials show absorption maxima located at around 390 nm, indicating that the electronic structure of the fluorescent precursor was not significantly perturbed in the ground state after the material preparation. The **DPM2** presents a photophysical behavior quite similar to the precursor in solution. The **DPM1** presents fluorescence emission red-shifted by 33 nm in spite of **DPM2**, which can be probably attributed to π–π stacking between the terephthalate cores. Any evidence of auto-organization could be observed in these materials.

Acknowledgements

We are grateful for financial support and scholarships from the Brazilian agencies CNPq and CAPES and Instituto Nacional de Inovação em Diagnósticos para a Saúde Pública (INDI-Saúde).

Notes and references

1 F. Hoffmann and M. Fröba, *Chem. Soc. Rev.*, 2011, **40**, 608.
2 U. A. Kober, M. R. Gallas, L. F. Campo, F. S. Rodembusch and V. Stefani, *J. Sol-Gel Sci. Technol.*, 2009, **52**, 305.
3 E. Poli, E. Merino, U. Díaz, D. Brunel and A. Corma, *J. Mater. Chem.*, 2011, **21**, 8524.
4 L. Zhao, M. Vaupel, D. A. Loy and K. J. Shea, *Chem. Mater.*, 2008, **20**, 1870.
5 H. Nam, B. Boury and S. Y. Park, *Chem. Mater.*, 2006, **18**, 5716.
6 L. Brigo, G. Grenci, L. Baù, A. Carpentiero, F. Mancin, F. Romanato, M. Tormen, M. Guglielmi and G. Brusatin, *Microelectron. Eng.*, 2011, **88**, 1913.
7 J. Liu, B. Yan and L. Guo, *Eur. J. Inorg. Chem.*, 2010, 2290.
8 W. Wang, J. E. Lofgreen and G. A. Ozin, *Small*, 2010, **6**, 2634.
9 H.-S. Xia, C.-H. Zhou, D. S. Tong and C. X. Lin, *J. Porous Mater.*, 2010, **17**, 225.
10 N. Mizoshita, K.-I. Yamanaka, T. Shimada, T. Tani and S. Inagaki, *Chem. Commun.*, 2010, **46**, 9235.
11 R. Corriu and T. A. Nguyên, *Molecular Chemistry of Sol–Gel derived Nanomaterials*, Wiley, Chichester, U.K., 1 edn, 2009.
12 J. J. E. Moreau, L. Vellutini, M. W. C. Man and C. Bied, *J. Am. Chem. Soc.*, 2001, **123**, 1509.
13 S. C. Nunes, N. J. O. Silva, J. Hummer, R. A. S. Ferreira, P. Almeida, L. D. Carlos and V. D. Bermudez, *RSC Adv.*, 2012, **2**, 2087.
14 J. Graffion, X. Cattoen, V. T. Freitas, R. A. S. Ferreira, M. W. C. Man and L. D. Carlos, *J. Mater. Chem.*, 2012, **22**, 6711.
15 L. D. Carlos, J. M. Pacheco, R. A. S. Ferreira and A. L. L. Videira, *Small*, 2010, **6**, 386.
16 L. D. Carlos, V. D. Bermudez, V. S. Amaral, S. C. Nunes, N. J. O. Silva, R. A. S. Ferreira, J. Rocha, C. V. Santilli and D. Ostrovskii, *Adv. Mater.*, 2007, **19**, 341.
17 F. Lerouge, G. Cerveau and R. J. P. Corriu, *New J. Chem.*, 2006, **30**, 1364.
18 A. Mehdi, C. Reye and R. Corriu, *Chem. Soc. Rev.*, 2011, **40**, 563.
19 L. F. Campo, F. S. Rodembusch, F. Lerouge, J. Alauzun, G. Cerveau and R. J. P. Corriu, *C. R. Chim.*, 2008, **11**, 1271.
20 D. Herault, F. Rodembusch, L. Campo, M. Gingras, G. Cerveau and R. J. P. Corriu, *C. R. Chim.*, 2010, **13**, 566.
21 L. Li, F. Cai, X. Sun and H. Peng, *Front. Chem. China*, 2010, **5**, 277.
22 J. J. E. Moreau, B. P. Pichon, M. W. C. Man, C. Bied, H. Pritzkow, J.-L. Bantignies, P. Dieudonné and J.-L. Sauvajol, *Angew. Chem., Int. Ed.*, 2004, **43**, 203.
23 M. A. Wahab, I. Kim and C. S. Ha, *J. Nanosci. Nanotechnol.*, 2008, **8**, 3532.
24 S. D. Ohmura, T. Moriuchi and T. Hirao, *Tetrahedron Lett.*, 2010, **51**, 3190.
25 R. Pflantz and J. Christoffers, *Chem.–Eur. J.*, 2009, **15**, 2200.
26 M. Shimizu, Y. Asai, Y. Takeda, A. Yamatani and T. Hiyama, *Tetrahedron Lett.*, 2011, **52**, 4084.
27 Y. Zhang, P. Starynowicz and J. Christoffers, *Eur. J. Org. Chem.*, 2008, 3488.
28 L. Shi and C. Wu, *Inorg. Chem. Commun.*, 2011, **14**, 569.
29 S. E. Page, W. A. Arnold and K. McNeill, *J. Environ. Monit.*, 2010, **12**, 1658.
30 U. Cernigoj, M. Kete and U. L. Stangar, *Catal. Today*, 2010, **151**, 46.
31 Y. Qian, S. Li, Q. Wang, X. Sheng, S. Wu, S. Wang, J. Li and G. Yang, *Adv. Mater.*, 2009, **21**, 3165.
32 D. D. Perrin and W. L. F. Armarego, *Purification of Laboratory Chemicals*, Pergamon Press, Oxford, 2nd edn, 1980.
33 A. T. Nielsen and W. R. Carpenter, *Org. Synth.*, 1965, **45**, 25.
34 K. Suzuki, A. Kobayashi, S. Kaneko, K. Takehira, T. Yoshihara, H. Ishida, Y. Shiina, S. Oishi and S. Tobita, *Phys. Chem. Chem. Phys.*, 2009, **11**, 9850.
35 R. E. Kellogg and R. G. Bennett, *J. Chem. Phys.*, 1964, **41**, 3042.
36 M. S. Wrighton, D. S. Ginley and D. L. Morse, *J. Phys. Chem.*, 1974, **78**, 2229.
37 M. J. Frisch, G. W. Trucks, H. B. Schlegel, G. E. Scuseria, M. A. Robb, J. R. Cheeseman, J. A. Montgomery, Jr., T. Vreven, K. N. Kudin, J. C. Burant, J. M. Millam, S. S. Iyengar, J. Tomasi, V. Barone, B. Mennucci, M. Cossi, G. Scalmani, N. Rega, G. A. Petersson, H. Nakatsuji, M. Hada, M. Ehara, K. Toyota, R. Fukuda, J. Hasegawa, M. Ishida, T. Nakajima, Y. Honda, O. Kitao, H. Nakai, M. Klene, X. Li, J. E. Knox, H. P. Hratchian, J. B. Cross, C. Adamo, J. Jaramillo, R. Gomperts, R. E. Stratmann, O. Yazyev, A. J. Austin, R. Cammi, C. Pomelli, J. W. Ochterski, P. Y. Ayala, K. Morokuma, G. A. Voth, P. Salvador, J. J. Dannenberg, V. G. Zakrzewski, S. Dapprich, A. D. Daniels, M. C. Strain, O. Farkas, D. K. Malick, A. D. Rabuck, K. Raghavachari, J. B. Foresman, J. V. Ortiz, Q. Cui, A. G. Baboul, S. Clifford,

J. Cioslowski, B. B. Stefanov, G. Liu, A. Liashenko, P. Piskorz, I. Komaromi, R. L. Martin, D. J. Fox, T. Keith, M. A. Al-Laham, C. Y. Peng, A. Nanayakkara, M. Challacombe, P. M. W. Gill, B. Johnson, W. Chen, M. W. Wong, C. Gonzalez and J. A. Pople, Gaussian Inc., Wallingford, CT, 2004.

38 R. Naef, *Dyes Pigm.*, 1991, **17**, 113.

39 M. K. Nayak and S. K. Dogra, *J. Photochem. Photobiol., A*, 2004, **161**, 169.

40 J. E. Kwon and S. Y. Park, *Adv. Mater.*, 2011, **23**, 3615.

41 T. Kanda, A. Momotake, Y. Shinohara, T. Sato, Y. Nishimura and T. Arai, *Bull. Chem. Soc. Jpn.*, 2009, **82**, 118.

42 T. Iijima, A. Momotake, Y. Shinohara, T. Sato, Y. Nishimura and T. Arai, *J. Phys. Chem. A*, 2010, **114**, 1603.

43 Z. R. Grabowski, K. Rotkiewicz and W. Rettig, *Chem. Rev.*, 2003, **103**, 3899.

44 J. Piechowska and D. T. Gryko, *J. Org. Chem.*, 2011, **76**, 10220.

45 S. K. Dogra, *J. Lumin.*, 2005, **114**, 101.

46 S. K. Dogra, *J. Lumin.*, 2005, **114**, 213.

47 D. LeGourriérec, V. A. Kharlanov, R. G. Brown and W. Rettig, *J. Photochem. Photobiol., A*, 2000, **130**, 101.

48 N. Basaric and P. Wan, *Photochem. Photobiol. Sci.*, 2006, **5**, 656.

49 K. A. Zachariasse, M. Grobys, T. von der Haar, A. Hebecker, Y. V. Il'ichev, Y. B. Jiang, O. Morawski and W. Kühnle, *J. Photochem. Photobiol., A*, 1996, **102**, 59.

50 J. R. Lakowicz, *Solvent and Environmental Effects, Principles of Fluorescence Spectroscopy*, Springer, New York, 2006, 3rd edn, pp. 207–210.

51 F. S. Santos, T. M. H. Costa, V. Stefani, P. F. B. Gonçalves, R. R. Descalzo, E. V. Benvenutti and F. S. Rodembusch, *J. Phys. Chem. A*, 2011, **115**, 13390.